The Organic Metal $(Me_2$–DCNQI$)_2$Cu: Dramatic Changes in Solid-State Properties and Crystal Structure Due to Secondary Deuterium Effects[1]

Klaus Sinzger,[2a] Siegfried Hünig,*[,2a] Martina Jopp,[2a] Dagmar Bauer,[2b] Werner Bietsch,[2b] Jost Ulrich von Schütz,*[,2b] Hans Christoph Wolf,[2b] Reinhard Karl Kremer,[2c] Tobias Metzenthin,[2d] Robert Bau,*[,2d] Saeed I. Khan,[2e] Andreas Lindbaum,[2f] Christian L. Lengauer,[2g] and Ekkehart Tillmanns*[,2g]

Contribution from the Institut für Organische Chemie der Universität Würzburg, Am Hubland, D-97074 Würzburg, Germany, 3. Physikalisches Institut, Universität Stuttgart, Pfaffenwaldring 57, D-70550 Stuttgart, Germany, Max Planck Institut für Festkörperforschung, Heisenbergstrasse 1, D-70569 Stuttgart, Germany, Chemistry Department, University of Southern California, Los Angeles, California 90089, J. D. McCullough X-ray Crystallography Laboratory, Department of Chemistry and Biochemistry, University of California, Los Angeles, California 90024, Institut für Experimentalphysik der TU Wien, Karlsplatz 13, A-1040 Wien, Austria, and Institut für Mineralogie und Kristallograhie der Universität Wien, Dr. Karl Lueger-Ring 1, A-1010 Wien, Austria

Received February 9, 1993

Abstract: Although $(R^1,R^3$–DCNQI$)_2$Cu salts (**1**) are isomorphic (space group $I4_1/a$), they behave differently upon cooling: The group M salts remain metallic down to the lowest temperatures, whereas the group M–I salts show phase transitions to semiconductors at temperatures T_{M-I} = 160–230 K. With regard to the steric requirements of the methyl group, **1a** ($CH_3/CH_3/H_2$) is expected to belong to group M–I, but it remains metallic even at 0.4 K (σ = 500 000 S cm^{-1}). Deuterated **1a**, however, namely **1c** ($CH_3/CD_3/H_2$), **1d** ($CD_3/CD_3/H_2$), and **1e** ($CD_3/CD_3/D_2$), undergo sharp phase transitions at 58, 73, and 82 K, respectively, the lowest phase-transition temperatures observed so far for copper salts **1** at ambient pressure. Thereby, conductivities drop by 6–8 orders of magnitude within a few kelvins, transforming **1c–e** from three-dimensional into strictly one-dimensional systems. This unprecedented strong secondary deuterium isotope effect is also reflected in significant changes in ESR signals and magnetic susceptibilities. Structure determinations by X-ray analysis of **1a** and **1d** at various temperatures (20 K, 156 K, and room temperature) reveal characteristic differences of the crystal structures above and below the phase-transition temperature T_{M-I} for both compounds. The very special structural features of the crystals are related to their 7-fold diamondoid superstructure, which includes infinite superhelices in the stacks of ligands and copper ions. A phase diagram of $(R^1,R^3$–DCNQI$)_2$Cu salts (**1**) is derived from a comparison of temperature-dependent structural and conductivity data, which shows that the conductive properties of the salts depend dramatically on the N–Cu–N angle α_{co}. A minimal threshold value ($\alpha_{co} \approx 126.4°$) is evaluated which determines the phase behavior of **1** upon cooling or applying pressure. In order to understand their unique properties as compared to those of other DCNQI metal salts, a new approach to DCNQI copper salts is presented in terms of a "two conductors in one" concept, which is a unique combination of a common one-dimensional (anisotropic) conduction path along segregated stacks and a three-dimensional (isotropic) conduction path within a Robin–Day class III network of delocalized mixed-valent metal ions bridged by organic spacers allowing electron transfer.

Introduction

In the rapidly growing field of organic conducting materials, radical anion salts of 2,5-disubstituted *N,N'*-dicyanoquinone diimines (DCNQIs) of the general structure $(R^1,R^3$–DCNQI$)_2$M (M = Li, Na, K, Rb, NH_4, Tl, Cu, Ag)[3] occupy a special position for several reasons: (1) The salts form black needles (single crystals) in which the cations are arranged like strings of pearls surrounded and connected by columns of DCNQI ligands. (2) Despite widespread variations of the substituents R^1 and R^3, the space groups either remain $I4_1/a$ (M = Li, Cu, Ag) or change to the closely related groups $C2/c$ (M = Na) and $P4/n$ (M = K, Rb, NH_4, Tl). (3) DCNQI salts with M = Li, Na, K, Rb, NH_4, Tl, and Ag form metal-like (cf. ref 4 for definition) semiconductors with conductivities of σ = 10–100 S cm^{-1} at ambient temperature. (4) Only the isomorphous salts $(R^1,R^3$–DCNQI$)_2$Cu (**1**) display metallic properties (quasi-three-dimensional) with σ = 100–1000 S cm^{-1} at ambient temperature. The Cu salts are classified into two groups according to the temperature dependence of their conductivities at ambient pressure: Group M salts (R^1/R^3 = Me/Me, Cl/I, Me/I, Br/I, I/I, Me/OMe, Br/OMe, I/OMe, OMe/OMe) show metallic behavior down to the lowest temperatures. Thereby the conductivity may increase to as much as 500 000 S cm^{-1} (R^1/R^3 = Me/Me).[5] Group M–I salts (R^1/R^3 = Cl/Cl, Cl/Me, Cl/Br, Br/Me, Br/Br, Cl/OMe) exhibit rather sharp metal–insulator transitions in the temperature range T_{M-I} = 160–230 K.

(1) Preliminary communications: (a) Hünig, S.; Sinzger, K.; Jopp, M.; Bauer, D.; Bietsch, W.; von Schütz, J. U.; Wolf, H. C. *Angew. Chem.* **1992**, *104*, 896; *Angew. Chem., Int. Ed. Engl.* **1992**, *31*, 859. (b) von Schütz, J. U.; Bair, M.; Bauer, D.; Bietsch, W.; Krebs, M.; Wolf, H. C.; Hünig, S.; Sinzger, K. *Proceedings of the International Conference on Synthetic Metals*, Göteborg, Sweden; Synthetic Metals; Elsevier Sequoia: Lausanne, Switzerland, 1992.

(2) (a) Universität Würzburg (syntheses and crystals); (b) Universität Stuttgart and (c) Max Planck Institut Stuttgart (solid-state properties); (d) University of Southern California and (e) University of California, Los Angeles (structure determinations); (f) TU Wien and (g) Universität Wien (temperature dependence of lattice constants).

(3) (a) Hünig, S.; Erk, P. *Adv. Mater.* **1991**, *3*, 225. (b) Hünig, S. *Pure Appl. Chem.* **1990**, *62*, 395.

(4) Miller, J. S.; Epstein, A. J. *Angew. Chem.* **1987**, *99*, 332; *Angew. Chem., Int. Ed. Engl.* **1987**, *26*, 287.

(5) Aumüller, A.; Erk, P.; Klebe, G.; Hünig, S.; von Schütz, J. U.; Werner, H.-P. *Angew. Chem.* **1986**, *98*, 759; *Angew. Chem., Int. Ed. Engl.* **1986**, *25*, 740.

0002-7863/93/1515-7696$04.00/0

Chart I. 2,5-(R^1,R^3-DCNQI)$_2$Cu Salts and Phase-Transition Temperatures $T_{M\text{-}I}$ from the Metallic (3d) to the Semiconducting (1d) State

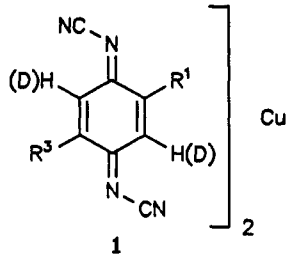

1

compd	R^1	R^3	H/D	$T_{M\text{-}I}$ [K]
1a	CH_3	CH_3	H	met.[a]
1a	CH_3	CH_3	H	47 (150 bar)[b]
1a	CH_3	CH_3	H	76 (400 bar)[b]
1b	CH_3	CH_3	D	met.[c,d]
1c	CD_3	CH_3	H	58[c]
1d	CD_3	CD_3	H	73[c]
1e	CD_3	CD_3	D	82[c]
1f	CH_3	I	H	met.[e]
1g	Br	I	H	met.[e]
1h	CH_3	Br	H	160[e]
1i	Br	Br	H	160[e]
1k	Cl	Br	H	205[e]
1l	Cl	CH_3	H	210[e]
1m	Cl	Cl	H	230[f]
1n	OCH_3	OCH_3	H	met.[e]

[a] From ref 5. [b] From ref 9a. [c] This work. [d] Instability of σ at 60 K. [e] From ref 6. [f] From ref 28c.

We now approach again a long-standing question[6] by conducting new experiments: How are variations of the substituents R^1 and R^3 in the DCNQI ligand translated into subtle structural differences in the corresponding copper salts **1** of the unchanged space group $I4_1/a$, thereby either allowing or preventing phase transitions upon cooling?

A thorough analysis of 15 differently substituted salts **1** with respect to ligand and solid-state properties[6,7] revealed that the size of the substituents is an essential factor governing the occurrence of phase transition upon cooling: Whereas combinations of small substituents (Cl and Br—even in combination with Me) induce phase transitions to metal-like semiconductors (group M–I salts), the large substituents OMe (except Cl/OMe) and I (iodine) maintain metallic conduction down to the lowest temperatures (group M salts). (2,5-Me_2-DCNQI)$_2$Cu, however, represents an exceptional case and cannot be described by this simplified scheme. Although the van der Waals volume of the Me group (22.7 Å^3)[8] is substantially smaller than that of Br (25.1 Å^3),[8] **1a** (CH_3/CH_3) does not undergo a phase transition down to 0.4 K, which contrasts with the behavior observed for **1h** (Me/Br) and **1i** (Br/Br) (Chart I).

Therefore, the electronic properties of the ligands were supposed to be crucial for the stability of the metallic state, too.[6] Indeed, the DCNQI ligands, the neutral molecules as well as the radical anions, reveal small, but distinct, differences in their electronic properties, i.e. higher LUMO and SOMO energies, respectively (ϵ_{LUMO} = –2.40 eV; ϵ_{SOMO} = –0.89 eV), and an enhanced donor strength of the CN group ($\epsilon_{\sigma n}$ = –22.03, –17.92 eV) for the ligand of **1a** as compared to those of **1h** (ϵ_{LUMO} = –2.64 eV; ϵ_{SOMO} = –1.14 eV; $\epsilon_{\sigma n}$ = –22.17, –18.10 eV) and **1i** (ϵ_{LUMO} = –2.84 eV; ϵ_{SOMO} = –1.37 eV; $\epsilon_{\sigma n}$ = –22.29, –18.27 eV).[6,7] The donor strength of the CN group is represented here by the AM1 energies of the localized σn orbitals. For the ligand of **1h** (Me/Br) the mean value of two nondegenerate σn orbitals is given for both the neutral molecule and the radical anion.

Since it is already known that phase transitions of **1a** can easily be induced by applying even low pressures (cf. Chart I),[9] **1a** seems to be already on the tilt to a phase transition. This assumption is supported by the very recent proposal of Kobayashi et al.[10] that the enhanced susceptibility in the metallic state of **1a** at low temperatures is due to insulating domains induced by some stress within the sample. Therefore, substituents with electronic properties similar to those present in **1a** but with a somewhat smaller volume may possibly trigger a phase transition upon cooling. Both the steric and the electronic requisites are met by the CD_3 group.

As a result of the lower zero-point energy, the mean as well as the maximum C–D bond length of CD_4 is less than that of the C–H bonds of CH_4 in the *gas phase* by 0.15% and 0.37%, respectively.[11] Correspondingly, the molar volume of *liquid* CD_4 relative to CH_4 at 100 K is about 1% less,[12] whereas the volume of the unit cell in the *crystalline* state at 70 K is found to be 1.5% less.[13] From this, the volume of the CD_3 group can be estimated to be 1.0–1.5% less than that of the CH_3 group in the region of 50–100 K.

Deuterated CT complexes and organic superconductors have already been prepared, although for different reasons. For *crystalline* CT complexes, shifts of the temperatures for structural phase transitions from 0.75[14] up to 15 K[15] were observed upon H/D exchange, the sign of the shift depending on the specific structure. For deuterated superconductors of the BEDT-TTF type the critical temperatures increased by 0.28 K up to 0.6 K.[16] For deuterated $(TMTSF)_2ClO_4$ a decrease of 0.13 K[17] was reported.

In all these cases, only small *quantitative* changes in an already present property were observed. In sharp contrast, we found dramatic *qualitative* effects in the deuterated copper salts **1c–e**, i.e. phase transitions from a metallic to a semiconducting state induced by deuteration (Chart I, Figure 1). Such a phenomenon, due to a secondary deuterium isotope effect amplified by a collective[18] of an "infinite" number of "layers" of DCNQI molecules, has not been reported so far.[19]

(6) Erk, P.; Meixner, H.; Metzenthin, T.; Hünig, S.; Langohr, U.; von Schütz, J. U.; Werner, H.-P.; Wolf, H. C.; Burkert, R.; Helberg, H. W.; Schaumburg, G. *Adv. Mater.* **1991**, *3*, 311. Recalculation of the published data led partly to some alterations which are used in this paper.

(7) (a) Sinzger, K. Ph.D. Thesis, University of Würzburg, 1993. (b) Hünig, S.; Sinzger, K. To be published.

(8) (a) van Krevelen, D. W. *Properties of Polymers*, 3rd ed. (completely revised); Elsevier: New York, 1990. (b) Bondi, A. *J. Phys. Chem.* **1964**, *68*, 441. (c) Bondi, A. *Physical Properties of Molecular Crystals, Liquids and Gasses*; Wiley: New York, 1968. The special position of **1a** is even more apparent with the application of this newer van der Waals volume.

(9) (a) Tomic, S.; Jérôme, D.; Aumüller, A.; Erk, P.; Hünig, S.; von Schütz, J. U. *J. Phys. C: Solid State Phys.* **1988**, *21*, L203. (b) Tomic, S.; Jérôme, D.; Aumüller, A.; Erk, P.; Hünig, S.; von Schütz. J. U. *Europhys. Lett.* **1988**, *5*, 553. (c) Tomic, S.; Jérôme, D.; Aumüller, A.; Erk, P.; Hünig, S.; von Schütz, J. U. *Synth. Met.* **1988**, *27*, B281. (d) Miyamoto, A.; Kobayashi, H.; Kato, R.; Kobayashi, A.; Nishio, Y.; Kajita, K.; Sasaki, W. *Chem. Lett.* **1992**, 115.

(10) Kagoshima, S.; Miyazaki, T.; Osada, T.; Saito, Y.; Wada, N.; Yano, H.; Takahashi, T.; Kanoda, K.; Kobayashi, H.; Kobayashi, A.; Kato, R. *Proceedings of the International Conference on Synthetic Metals*, Göteborg, Sweden; Synthetic Metals; Elsevier Sequoia: Lausanne, Switzerland, 1992.

(11) Bartell, L. S.; Kuchitsu, K.; deNeui, R. J. *J. Chem. Phys.* **1961**, *35*, 1211.

(12) Fuks, S.; Legros, J.-C.; Bellemans, A. *Physica* **1965**, *31*, 606.

(13) Greer, S. C.; Meyer, L. *J. Chem. Phys.* **1970**, *52*, 468.

(14) Cooper, J. R.; Lukatela, J.; Miljak, M.; Fabre, J. M.; Giral, L.; Aharon-Shalom, E. *Solid State Commun.* **1978**, *25*, 949.

(15) Dalal, N. S.; Haley, L. V.; Northcott, D. J.; Park, J. M.; Reddoch, A. H.; Ripmeester, J. A.; Williams, D. F. *J. Chem. Phys.* **1980**, *73*, 2515.

(16) (a) Heidmann, C.-P.; Andres, K.; Schweitzer, D. *Physica* **1986**, *143B*, 357. (b) Oshima, K.; Uruyama, H.; Yamochi, H.; Saito, G. *J. Phys. Soc. Jpn.* **1988**, *57*, 730.

(17) Schwenk, H.; Hess, E.; Andres, K.; Wudl, F.; Aharon-Shalom, E. *Phys. Lett. A* **1984**, *102*, 57.

(18) For properties induced by collectives of molecules see: Menger, F. M. *Angew. Chem.* **1991**, *103*, 1104; *Angew. Chem., Int. Ed. Engl.* **1991**, *30*, 1086.

(19) On the basis of a personal communication from S.H. to A. Kobayashi (3/19/1992), 2,5-Me_2-DCNQI-d_7 and copper/lithium alloys (2,5-Me_2-DCNQI-d_7)$_2$Cu$_{1-x}$Li$_x$ have been prepared.[37] The sharp phase transition at 75 K (x = 0) is suppressed for x = 0.20.

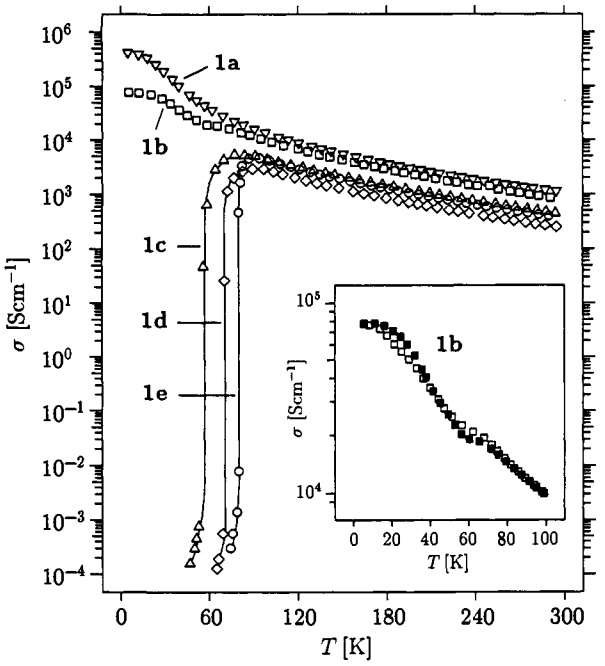

Figure 1. Temperature dependence of the conductivity σ of **1a** ($CH_3/CH_3/H_2$), **1b** ($CH_3/CH_3/D_2$), **1c** ($CH_3/CD_3/H_2$), **1d** ($CD_3/CD_3/H_2$), and **1e** ($CD_3/CD_3/D_2$). Insert shows expanded detail of the conductivity of **1b** below 100 K: closed squares, cooling; open squares, warming.

Results and Discussion

Deuterated Salts 1b–e and Their Solid-State Properties. Whereas substitution of one CH_3 group of **1a** to yield **1c** ($CH_3/CD_3/H_2$) induces a sharp phase transition at 58 K (Figure 1), substitution of both CH_3 groups to produce **1d** ($CD_3/CD_3/H_2$) triggers this conversion at 73 K. Additionally, exchanging the ring hydrogen atoms of **1d** to yield **1e** ($CD_3/CD_3/D_2$) shifts the phase transition to the higher temperature 82 K. As the phase transitions take place, conductivities drop by 6–8 orders of magnitude (!) within a few kelvins. Below T_{M-I} the conductivities become activated at ≈900 K (≈80 meV), a value typical for one-dimensional systems. Deuteration of only the ring hydrogen atoms in **1a** to produce **1b** ($CH_3/CH_3/D_2$) does not induce a phase transition at low temperatures, although an instability of σ results with a slight hysteresis between the cooling and the heating cycle, respectively, at about 60 K (Figure 1 insert).

Although DCNQI copper salts usually exhibit high static susceptibility within the metallic region, an ESR signal is not detectable due to the three-dimensional movement of the electrons. Strong spin–orbit coupling and exchange between the conduction electrons and the Cu d states lead to extreme line widths. Below the phase-transition temperature T_{M-I} (e.g. for **1h** or **1i**), rather broad ESR signals develop which narrow upon further cooling.[20] Salts **1c–e**, however, behave quite differently: below T_{M-I}, ESR signals (ΔB_{pp} (2–3) × 10^{-3} T) appear with line widths at least 1 order of magnitude more narrow than the known examples and with only a weak temperature dependence (Figure 2). This behavior is indicative of systems with isolated spins or one-dimensional systems. Since there is no characteristic g = 2.00 signal below T_{M-I}, the spins on the DCNQI stacks must pair in coincidence with the disappearance of the conductivity. The virtual loss of the DCNQI charge carriers is in accordance with the extreme switchlike decrease of the conductivity at T_{M-I}. Concomitantly, there is no longer mixing of the charge carrier spins and the Cu^{2+} spins, which is responsible for the ESR silence above the phase transition. Hence, the (now localized) Cu^{2+} spins become detectable with a g-factor anisotropy of $g_{\parallel}$ = 2.41 and $g_{\perp}$ = 2.08, values known for Cu^{2+} states in a ligand field with a distorted tetrahedral symmetry.[21] Below 8 K the ESR signal vanishes due to an antiferromagnetic ordering (AFO). In contrast to the case for **1l** (Cl/CH_3),[22] however, no antiferromagnetic resonance signal is observed at temperatures as low as 4.2 K. In $\chi(T)$, the AFO is indicated by a decrease below 8 K (Figure 2). This ordering is a common feature for group M–I salts,[22,23a] but it is also found in **1a**.[23] Above the temperature range of Figure 2, the static susceptibility is independent of temperature as high as room temperature.

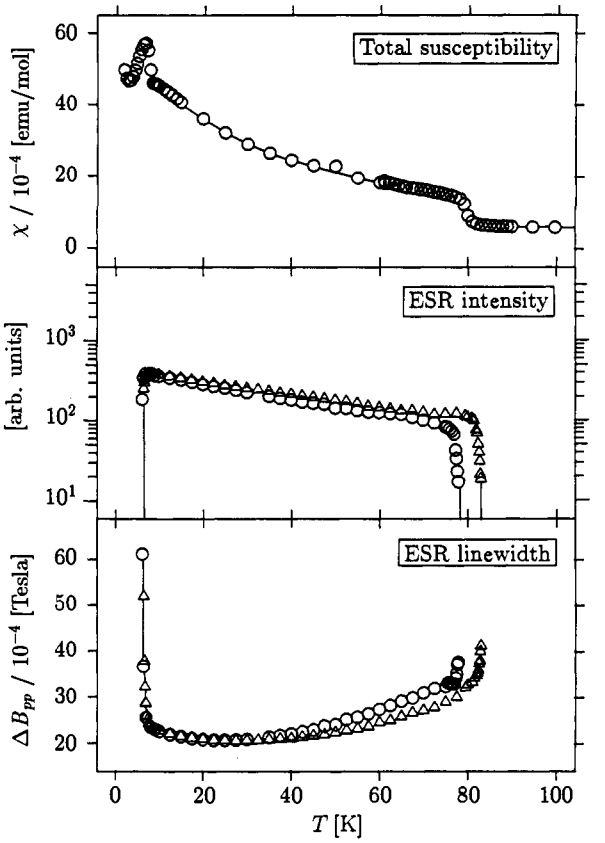

Figure 2. Temperature dependences of the total susceptibility (SQUID) at B = 0.1 T (not corrected by the diamagnetic contribution), of the intensity of the ESR signal (ESR susceptibility), and of the ESR line width ΔB_{pp} for **1e** ($CD_3/CD_3/D_2$) in a restricted temperature range: circles, cooling; triangles, warming. The ESR susceptibility is a direct measure for only the paramagnetic component of the total susceptibility.

Crystal Structures of the Nondeuterated Salt 1a and of the Deuterated Salt 1d at Various Temperatures. The striking changes in solid-state properties of **1c–e** demonstrated above should be connected with subtle structural differences above, and somewhat more pronounced deviations below, the phase-transition temperature as compared to the case of **1a**. To trace these features, X-ray investigations at various temperatures were performed with **1d** and, for comparison under the same conditions, with **1a**.[24] Copper salts **1a** and **1d** (and also **1c**[25]) are isomorphous at room

(20) von Schütz, J. U.; Werner, H.-P.; Wolf, H. C.; Aumüller, A.; Erk, P.; Hünig, S. *Magn. Reson. Relat. Phenom., Proc. Congr. Ampere, 23rd* **1986**, 158.

(21) (a) Hathaway, B. J. In *Comprehensive Coordination Chemistry*; Wilkinson, G., Gillard, R. D., McCleverty, J. A., Eds.; Pergamon Press: New York, 1987; Vol. 5, pp 533–774. (b) Sharnoff, M. *J. Chem. Phys.* **1965**, *42*, 3383.

(22) (a) Werner, H.-P.; von Schütz, J. U.; Wolf, H. C.; Kremer, R.; Gehrke, M.; Aumüller, A.; Erk, P.; Hünig, S. *Solid State Commun.* **1988**, *65*, 809. (b) Burkert, R.; Helberg, H. W.; von Schütz, J. U. *Proceedings of the International Conference on Synthetic Metals*, Göteborg, Sweden; Synthetic Metals; Elsevier Sequoia: Lausanne, Switzerland, 1992.

(23) (a) Kobayashi, H.; Kato, R.; Kobayashi, A.; Mori, T.; Inokuchi, H. *Solid State Commun.* **1988**, *65*, 1351. (b) Kagoshima, S.; Sugimoto, N.; Osada, T.; Kobayashi, A.; Kato, R.; Kobayashi, H. *J. Phys. Soc. Jpn.* **1991**, *60*, 4222.

(24) The structure of **1a** is already known.[5,23a]

Table I. Summary of Crystal Data for Salts 1a and 1d at Various Temperatures[25] (Space group $I4_1/a$, $Z = 4$)

salt	**1a** (RT)	**1a** (20 K)[a]	**1d** (RT)	**1d** (156 K)[a]	**1d** (20 K)[a]
crystal dimens mm	0.45 × 0.20 × 0.20	0.45 × 0.20 × 0.20	0.50 × 0.10 × 0.08	0.50 × 0.10 × 0.08	0.50 × 0.10 × 0.08
cell dimens					
a, Å	21.606(2)	21.654(5)	21.619(2)	21.63(1)	21.693(3)
c, Å	3.8811(4)	3.792(1)	3.8744(4)	3.799(2)	3.776(1)
V, Å^3	1811.7(3)	1778.0(7)	1810.8(3)	1776.9(15)	1776.7(6)
d_{calc}, g/cm^3	1.58	1.61	1.58	1.61	1.61
linear abs coeff, cm^{-1}	12.31	12.55	12.56	12.55	12.56
scan mode	$\theta/2\theta$	$\theta/2\theta$	$\theta/2\theta$	$\theta/2\theta$	$\theta/2\theta$
scan speed, deg/min	12.0	6.0	6.0	6.0	6.0
2θ range, deg	1–60	1–60	1–60	1–60	1–60
tot. no. of obsd reflns	2780	2720	1633	1554	3106
no. of unique data with $\|F_o\| \geq 3\sigma(F_o)$	978	1160	850	1043	988
no. of param	78	78	78	78	78
R	0.042	0.031	0.042	0.043	0.031

[a] Estimated standard deviations of temperature: 20 ± 2 and 156 ± 3 K.

Table II. Fractional Atomic Coordinates and Equivalent Isotropic Thermal Parameters (Å^2), with Esd's of the Refined Parameters in parentheses for 1a at Room Temperature

atom	x/a	y/b	z/c	10^4U_{eq}[a]
Cu	0.0000	0.2500	0.6250	265(2)
N(1)	–0.0354(1)	0.3233(1)	0.8617(6)	312(11)
N(2)	–0.0715(1)	0.4225(1)	1.1053(5)	288(11)
C(1)	–0.0491(1)	0.3703(1)	0.9824(7)	266(12)
C(2)	–0.0359(1)	0.4593(1)	1.2980(7)	260(12)
C(3)	–0.0626(1)	0.5167(1)	1.4188(6)	257(12)
C(4)	0.0270(1)	0.4448(1)	1.3871(7)	262(12)
C(5)	–0.1287(1)	0.5323(1)	1.3332(9)	353(15)
H(4)	0.043(2)	0.407(2)	1.311(10)	322[b]
H(5A)	–0.140(2)	0.526(2)	1.120(12)	430[b]
H(5B)	–0.153(2)	0.507(2)	1.422(12)	430[b]
H(5C)	–0.142(2)	0.567(2)	1.439(11)	430[b]

[a] $U_{eq} = [1/(6\pi^2)]\sum_i\sum_j\beta_{ij}a_ia_j$. [b] Temperature factor not refined.

Table III. Fractional Atomic Coordinates and Equivalent Isotropic Thermal Parameters (Å^2), with Esd's of the Refined Parameters in Parentheses, for 1a at 20 K

atom	x/a	y/b	z/c	10^4U_{eq}[a]
Cu	0.0000	0.2500	0.6250	49(1)
N(1)	–0.0369(1)	0.3224(1)	0.8597(3)	80(6)
N(2)	–0.0722(1)	0.4230(1)	1.0961(3)	71(6)
C(1)	–0.0502(1)	0.3702(1)	0.9772(4)	73(6)
C(2)	–0.0362(1)	0.4595(1)	1.2940(4)	64(6)
C(3)	–0.0626(1)	0.5173(1)	1.4160(4)	67(6)
C(4)	0.0263(1)	0.4445(1)	1.3864(4)	67(6)
C(5)	–0.1285(1)	0.5327(1)	1.3286(4)	81(6)
H(4)	0.042(1)	0.410(2)	1.311(8)	127[b]
H(5A)	–0.135(1)	0.532(2)	1.082(8)	127[b]
H(5B)	–0.155(1)	0.505(2)	1.428(8)	127[b]
H(5C)	–0.141(1)	0.569(2)	1.438(8)	127[b]

[a] $U_{eq} = [1/(6\pi^2)]\sum_i\sum_j\beta_{ij}a_ia_j$. [b] Temperature factor not refined.

Table IV. Fractional Atomic Coordinates and Equivalent Isotropic Thermal Parameters (Å^2), with Esd's of the Refined Parameters in Parentheses for 1d at Room Temperature

atom	x/a	y/b	z/c	10^4U_{eq}[a]
Cu	0.0000	0.2500	0.6250	241(2)
N(1)	–0.0356(1)	0.3232(1)	0.8627(7)	277(13)
N(2)	–0.0714(1)	0.4224(1)	1.1039(6)	267(13)
C(1)	–0.0492(1)	0.3700(1)	0.9845(8)	231(14)
C(2)	–0.0360(1)	0.4593(1)	1.2978(7)	215(14)
C(3)	–0.0626(1)	0.5166(1)	1.4197(7)	229(14)
C(4)	0.0269(1)	0.4447(1)	1.3869(8)	239(14)
C(5)	–0.1285(1)	0.5321(2)	1.3344(10)	322(17)
H(4)	0.044(2)	0.410(2)	1.314(12)	380[b]
H(5A)	–0.141(2)	0.526(2)	1.114(13)	380[b]
H(5B)	–0.156(2)	0.504(2)	1.393(12)	380[b]
H(5C)	–0.141(2)	0.566(2)	1.415(12)	380[b]

[a] $U_{eq} = [1/(6\pi^2)]\sum_i\sum_j\beta_{ij}a_ia_j$. [b] Temperature factor not refined.

Table V. Fractional Atomic Coordinates and Equivalent Isotropic Thermal Parameters (Å^2), with Esds of the Refined Parameters in Parentheses, for **1d** at 156 K

atom	x/a	y/b	z/c	10^4U_{eq}[a]
Cu	0.0000	0.2500	0.6250	104(2)
N(1)	–0.0366(1)	0.1776(1)	0.8608(6)	129(10)
N(2)	–0.0720(1)	0.0773(1)	1.0981(6)	131(10)
C(1)	–0.0499(1)	0.1300(1)	0.9784(7)	111(11)
C(2)	–0.0362(1)	0.0406(1)	1.2963(6)	104(11)
C(3)	–0.0626(1)	–0.0172(1)	1.4179(7)	108(11)
C(4)	0.0268(1)	0.0554(1)	1.3858(7)	114(11)
C(5)	–0.1286(1)	–0.0323(1)	1.3307(8)	151(13)
H(4)	0.041(2)	0.091(2)	1.313(14)	253[b]
H(5A)	–0.138(2)	–0.031(2)	1.084(14)	253[b]
H(5B)	–0.155(2)	–0.005(2)	1.409(14)	253[b]
H(5C)	–0.140(2)	–0.067(2)	1.401(13)	253[b]

[a] $U_{eq} = [1/(6\pi^2)]\sum_i\sum_j\beta_{ij}a_ia_j$. [b] Temperature factor not refined.

temperature with space group $I4_1/a$. Despite the phase transition of **1d**, no gross changes in space group or lattice constants were found at 20 K with the single-crystal diffractometer. Therefore, the average[26] crystal structure (space group $I4_1/a$) was determined for **1d**. Crystal data are summarized in Table I. Final fractional coordinates and isotropic thermal parameters are given in Tables II–VI.

At room temperature the deuterated salt **1d** exhibits a somewhat shorter c-axis and slightly longer a- and b-axes in comparison to **1a** (Table I), a result also obtained from a determination of the lattice constants by the powder method.[27] Previously, Kobayashi et al.[23,28] found that the a- and b-axes are elongated slightly upon cooling while the c-axis shows normal thermal contraction. Due to the differences between C–D bonds and C–H bonds (vide supra), the changes of the lattice constants between room temperature and 20 K (expressed in percentages) for **1d** (+0.34% for a, b; –2.55% for c) are somewhat greater than those for **1a** (+0.22% for a, b; –2.30% for c). Similar to the crystals of other DCNQI copper salts, those of **1a** and **1d** can be described in terms of uniformly arranged one-dimensional columns of planar DCNQI acceptor molecules along the c-axis. Four acceptor

(25) The room-temperature structure of **1c** was also determined. Due to difficulties pertaining to apparatus, the accuracy of the obtained data is not as good as for salts **1a** and **1d**: ω-scan, space group $I4_1/a$, $Z = 4$, number of unique data with $|F_o| \geq 3\sigma(F_o) = 641$, $R = 0.047$, a, $b = 21.61(11)$ Å, $c = 3.84(1)$ Å, $V = 1792(14)$ Å^3, $\alpha_{fr} = 116.3(4)°$, $\alpha_{oo} = 124.8(5)°$.

(26) A 3-fold superstructure was identified by oscillation photographs and scanning of X-ray diffraction profiles of selected reflections for **1l** (Cl/CH$_3$) and **1h** (Br/CH$_3$): (a) Reference 23a. (b) Moret, R. *Synth. Met.* **1988**, *27*, B301. The development of these 3-fold superstructures is interpreted as an ordering of localized Cu$^+$ and Cu^{2+} ions in the ratio of 2:1. Nevertheless, only average crystal structures could be derived by usual X-ray analysis due to the weakness of the superstructure reflections.

(27) **1a**: a, $b = 21.607(1)$ Å, $c = 3.8823(6)$ Å, $V = 1812.5(3)$ Å^3, $\alpha_{fr} = 115.67(1)°$. **1d**: a, $b = 21.628(2)$ Å, $c = 3.8730(6)$ Å, $V = 1811.7(4)$ Å^3, $\alpha_{fr} = 115.84(2)°$.

(28) (a) Kobayashi, A.; Kato, R.; Kobayashi, H.; Mori, T.; Inokuchi, H. *Solid State Commun.* **1987**, *64*, 45. (b) Kobayashi, A.; Mori, T.; Inokuchi, H.; Kato, R.; Kobayashi, H. *Synth. Met.* **1988**, *27*, B275. (c) Kato, R.; Kobayashi, H.; Kobayashi, A. *J. Am. Chem. Soc.* **1989**, *111*, 5224.

Table VI. Fractional Atomic Coordinates and Equivalent Isotropic Thermal Parameters (Å^2), with Esd's of the Refined Parameters in Parentheses, for 1d at 20 K

atom	x/a	y/b	z/c	10^4U_{eq}[a]
Cu	0.0000	0.2500	0.6250	61(1)
N(1)	−0.0368(1)	0.3229(1)	0.8510(5)	125(8)
N(2)	−0.0720(1)	0.4230(1)	1.0911(5)	89(8)
C(1)	−0.0500(1)	0.3705(1)	0.9700(5)	90(9)
C(2)	−0.0359(1)	0.4597(1)	1.2909(5)	75(9)
C(3)	−0.0627(1)	0.5170(1)	1.4168(5)	71(8)
C(4)	0.0265(1)	0.4448(1)	1.3833(5)	76(8)
C(5)	−0.1285(1)	0.5320(1)	1.3291(5)	79(9)
H(4)	0.041(1)	0.409(1)	1.303(9)	127[b]
H(5A)	−0.135(1)	0.530(1)	1.098(10)	127[b]
H(5B)	−0.154(1)	0.504(1)	1.422(10)	127[b]
H(5C)	−0.138(1)	0.569(1)	1.426(9)	127[b]

[a] $U_{eq} = [1/(6\pi^2)]\sum_i\sum_j\beta_{ij}a_ia_j$. [b] Temperature factor not refined.

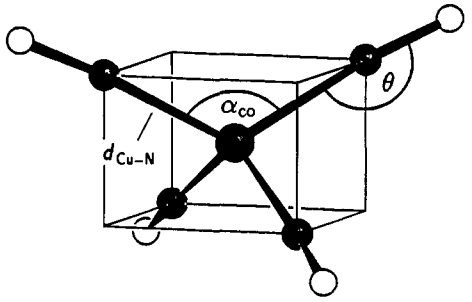

Figure 3. Geometry of the nitrile groups coordinated to the copper ion in (2,5-R^1,R^3–DCNQI)$_2$Cu.

molecules surround the copper cations on the $\bar{4}$ axis in a distorted tetrahedral arrangement (vide infra). The interplanar distances between the least-squares planes of the six-membered rings of the DCNQI units (including the imino nitrogen atoms) are in the ranges 3.208–3.213 Å at room temperature and 3.122–3.145 Å at 20 K. The molecular geometries of the DCNQI unit are essentially identical at room temperature as well at 20 K. At low temperatures, only the distances between the imino nitrogen and the nitrile carbon atom differ slightly in **1a** and **1d**. Significant changes, however, take place in the coordination sphere of the copper salts **1** with cooling. The most important coordination parameters (d_{Cu-N}, α_{co}, and θ; see Figure 3) are given in Table VII. Within experimental error, **1a** and **1d** exhibit almost the same coordination geometry at room temperature, while structural differences between these compounds emerge with cooling. In general, the N–Cu–N angle (α_{co}) increases as the temperature decreases (flattening of the coordination tetrahedron), while the Cu–N distances contract slightly. A more pronounced effect is seen with salt **1d**, for which the coordination angle at 20 K [α_{co} = 128.5(1)°] differs significantly from the corresponding α_{co} value of **1a** [126.3(1)°]. The overall increases of α_{co} between room temperature and 20 K are 1.5° for **1a** and 3.7° for **1d**, respectively. The Cu–N bond distance at 20 K is also somewhat shorter for **1d** [1.966(2) Å] than for **1a** [1.972(1) Å].

The variation of the Cu–N–C angle (θ) upon cooling does not show a uniform trend. While θ first decreases for both **1a** and **1d**, it increases again for **1d** after the phase transition. Likewise, a decrease of θ between room temperature and 100 K was described for copper salts without a phase transition, while θ remained virtually unaffected in copper salts exhibiting a metal–insulator transition.[28c]

The following discussion is based on the recent discovery of a 7-fold superdiamond architecture[29a] in the DCNQI copper salts **1**. The bidentate DCNQI units are coordinated in a distorted tetrahedral fashion to the copper ions, and a three-dimensional polymeric network is formed in which the copper ions build up a framework of seven interpenetrating diamond lattices. The smallest closed units composing the diamond lattice are adamantanoid Cu_{10} clusters (Figure 4), and the whole architecture is therefore best represented by the 7-fold adamantanoid superstructure of Figure 5. Closer inspection of Figure 4 reveals that both the copper ions on the top and bottom of this adamantanoid unit belong to the same column of copper ions piled along the *c*-axis of the crystal lattice. Going from the highest to the lowest copper ion via the ligands follows one helical turn. Within the 7-fold adamantanoid superstructure of Figure 5, four DCNQI stacks associated with four neighboring stacks of copper ions form a superhelix of seven intertwined single helices[29b] whose spacing in the direction of the stacking axis has the value of the cell lattice constant *c*. Hence, the high compressibility in the direction of stacking (lattice constant *c*) and the expansion of the lattice constants *a* and *b* upon cooling can be interpreted in terms of applying pressure to an ordinary elastic spring. A similar feature concerning the lattice constants can be observed at room temperature upon going from **1a** to **1d** (vide supra). Thus, H/D exchange can be considered as an equivalent to the application of pressure. Indeed, with an increasing degree of deuteration the temperature of phase transition rises, as it does with increasing pressure (Chart I).

The concept of a superdiamond architecture also provides a powerful tool to derive supermolecular geometrical crystal parameters in order to characterize the structural features of these radical anion salts. As shown in Figure 4, three DCNQI-bridged copper ions form a Cu–Cu–Cu angle α_{fr}, which is an important measure for the tetragonal compression within the framework of copper ions. As the latter are situated on special positions, their interatomic distances as well as α_{fr} are closely related to the lattice constants in the following way:

$$\alpha_{fr} = 2\arctan(2a/7c) \quad (1)$$

$$d_{Cu-Cu} = \frac{\sqrt{(a/2)^3 + (7c/4)^2}}{\sqrt{(a/2)^2 + (7c/4)^2}} \quad (2)$$

Though α_{co} and α_{fr} are not directly related, an inspection of Figure 4 reveals that both parameters should be influenced in a parallel way. Indeed, a correlation between α_{co} and α_{fr} was found[7] for a wide range of substituent combinations (vide infra). Since α_{fr} can be determined very exactly from the lattice constants (standard deviation 0.01–0.06°), it will better reflect subtle changes in the crystal lattice than the values of α_{co} (standard deviation 0.1–0.2°). Indeed, while α_{co} has equal values for **1a** and **1d** at room temperature, the values of α_{fr} reveal the somewhat higher tetragonal compression (by 0.12°) of **1d** as compared to **1a** (Table VII and ref 27).

In order to confirm the subtle differences found in unit cell parameters and tetragonal compression of the copper framework between salt **1a** and **1d** by single-crystal X-ray analysis, unit cell parameters of **1a** and **1d** were determined over the whole temperature range of interest here (4–300 K) by X-ray powder diffraction. Plots of the refined lattice constants *a* and *c*, of the unit cell volumes *V*, and of the angles α_{fr} are shown in Figure 6. Angles α_{fr} were calculated from the lattice constants according to eq 1. The following essential features can be derived from Figure 6: (1) Within the uncertainty of the method, lattice constants *a* are nearly the same for **1a** and **1d** over the whole temperature range and increase only very slightly upon cooling (≈0.1%, a somewhat smaller increase than that determined for the single crystal; vide supra). (2) A pronounced decrease (≈2.0%), however, can be observed for the lattice constant *c*, the *c* value of **1d** on an average being slightly but significantly smaller than that of **1a**. (3) The unit cell volume *V* reveals a behavior similar to that of lattice constant *c*. Furthermore, the difference

(29) (a) Ermer, O. *Adv. Mater.* **1991**, *3*, 608. (b) Similar helix structures have been described for other superdiamond lattices: Ermer, O.; Lindenberg, L. *Chem. Ber.* **1990**, *123*, 1111.

Table VII. Interplanar Distances within the DCNQI Columns and Coordination and Lattice Geometry of Cu in Salts 1a and 1d at Various Temperatures

salt	**1a** (RT)	**1a** (20 K)	**1d** (RT)	**1d** (156 K)	**1d** (20 K)
$d_{\pi-\pi}$, Å	3.213	3.145	3.208	3.154	3.122
α_{co} (∠N–Cu–N), deg	124.8(1)	126.3(1)	124.8(2)	125.9(1)	128.5(1)
d_{Cu-N}, Å	1.984(2)	1.972(1)	1.986(2)	1.970(2)	1.966(2)
θ (∠Cu–N–C), deg	170.6(2)	168.7(1)	170.6(2)	168.9(2)	169.3(2)
α_{fr} (∠Cu–Cu–Cu), deg	115.68(1)	116.99(2)	115.80(1)	116.83(6)	117.30(2)
d_{Cu-Cu}, Å	12.76	12.70	12.76	12.70	12.70

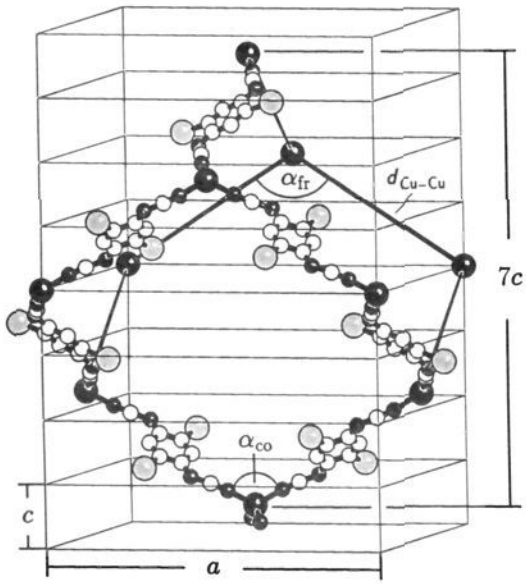

Figure 4. View of a single adamantanoid Cu_{10} cluster as part of the crystal lattice of (2,5-R^1,R^3–DCNQI)$_2$Cu (space group $I4_1/a$). The DCNQI ligands are partially replaced by "Cu–Cu bonds".

in volumes between **1a** and **1d** increases at lower temperatures. (4) As a consequence of the features observed for the lattice constants a and c, the tetragonal compression of the copper framework increases upon cooling, that of **1d** on the average being slightly but significantly larger than that of **1a**. From the explanations of the deuterium isotope effect of methane, the helices in the superstructure of **1d** ($CD_3/CD_3/H_2$) are expected to form more "compliant" springs[30] upon cooling as compared to the helices of **1a**. The temperature dependence of the cell volume V seems to support this assumption of a higher compressibility of **1d**. Unfortunately, the data of Figure 6 are not sufficiently precise to allow a final decision.

Besides, two further features are noteworthy: (5) Lattice constant c, unit cell volume V, and the tetragonal compression reach a plateau or even a smooth minimum (c, V)/maximum (α_{fr}), respectively, just below 50 K, a feature recently reported by another group[23b] and presumed to be responsible for the reentrance behavior of **1a** in the low-pressure regime. (6) Contrary to the observation of discontinuous changes of the lattice constants for other group M–I salts **1** at T_{M-I}[23,28] and despite the distinct decrease of the ligand coordination angle α_{co} in the single crystal of **1d** below T_{M-I} (Table VII), no discontinuous change of the unit cell parameters or the tetragonal compression was found for the microcrystalline material of **1d**.

Assuming that the deuterated methyl group has almost the same electronic properties as the ordinary methyl group (though a somewhat less effective electron release of the C–D bond as compared to the C–H bond was suggested by Halevi et al.[31]), the observed structural changes at low temperature must be attributed to small steric differences in the substituent size. Although the differences in the C–H and C–D bond distances cannot be determined directly by X-ray diffraction, we assume that the steric demands of the two substituents CH_3 and CD_3, respectively, due to the above-mentioned deviations of bond lengths of CH_4 and CD_4, should be different, as should atomic displacements due to molecular vibrational and lattice vibrational effects.

A Critical Coordination Angle α—The Key to the Metallic State of DCNQI Copper Salts. Shortly after the discovery of the copper salts **1**, several authors[9c,23a] assumed that their unique properties were due to a quasi-three-dimensional character, i.e. a pπ–d mixing arising from the mixed-valence state of the copper ions. It was further noticed that the phase behavior of the copper salts **1** must closely be related to the distortion of the tetrahedral geometry around the copper ion, which is reflected by the coordination angle α_{co}.[9c,23a] Both features will be taken into consideration in the following discussion.

As already mentioned in the beginning, we are dealing with a unique combination of two different conduction paths within the copper salts **1**. One of these paths is the well-known one-dimensional (anisotropic) conduction along stacks of uniformly arranged organic units in compounds with only partial charge transfer. This is the common feature for most of the TTF-type radical cation salts and also for most of the DCNQI metal salts (except for M = Cu). These one-dimensional systems are known to undergo charge density wave (CDW)- and/or spin density wave (SDW)-induced phase transitions. The other conduction path can be observed in materials which are characterized by a two- or three-dimensional network of mixed-valent metal ions bridged either by single atoms like oxygen or sulfur or by certain organic spacers.

Already in the late 1960s, Robin and Day[32] suggested a classification of these mixed-valence materials into three classes. Class I materials are characterized by very different geometries (for instance, different coordination numbers) at metal centers with localized, i.e. distinguishable, oxidation states. These compounds are insulators. Class III materials are characterized by identical stereochemistries at metal centers with completely delocalized, i.e. indistinguishable, oxidation states. These materials behave as two- or three-dimensional conductors. Class II occupies an intermediate position between class I and class III; i.e., these compounds are characterized by similar stereochemistries (differing from one another by slight distortions) at metal centers with (more or less) localized, distinguishable oxidation states. For these materials, which are semiconductors, formation of a superlattice is predicted.[32c]

Copper 1+/2+ mixed valency is a common feature in copper chemistry.[21a] Though most mixed-valent copper compounds belong to class I or II (e.g. $Cu^I_2Cu^{II}$(2,5-dithiahexane)$_6(ClO_4)_4$[34] or Cu^ICu^{II}(4-methylthiazole)$_4Cl_3$[35]), a few class III compounds are also known (e.g. KCu_4S_3[33]). The characteristics of class III

(30) This idea has been suggested by one of the reviewers.
(31) (a) Halevi, E. A. *Prog. Phys. Org. Chem.* **1963**, *1*, 866. (b) Halevi, E. A.; Nussim, M.; Ron, A. *J. Chem. Soc.* **1963**, 866.

(32) (a) Robin, M. B.; Day, P. *Adv. Inorg. Chem. Radiochem.* **1967**, *10*, 248. (b) Day, P. *Int. Rev. Phys. Chem.* **1980**, *1*, 149. (c) Day, P. In *Chemistry and Physics of One-Dimensional Metals*; Keller, H. J., Ed.; Plenum Press: New York, 1977; pp 197–223.
(33) Brown, D. B.; Zubieta, J. A.; Vella, P. A.; Wrobleski, J. T.; Watt, T.; Hatfield, W. E.; Day, P. *Inorg. Chem.* **1980**, *19*, 1945.
(34) Olmstead, M. M.; Musker, W. K.; Kessler, R. M. *Inorg. Chem.* **1981**, *20*, 151.
(35) Marsh, W. E.; Hatfield, W. E.; Hodgson, D. J. *Inorg. Chem.* **1983**, *22*, 2899.

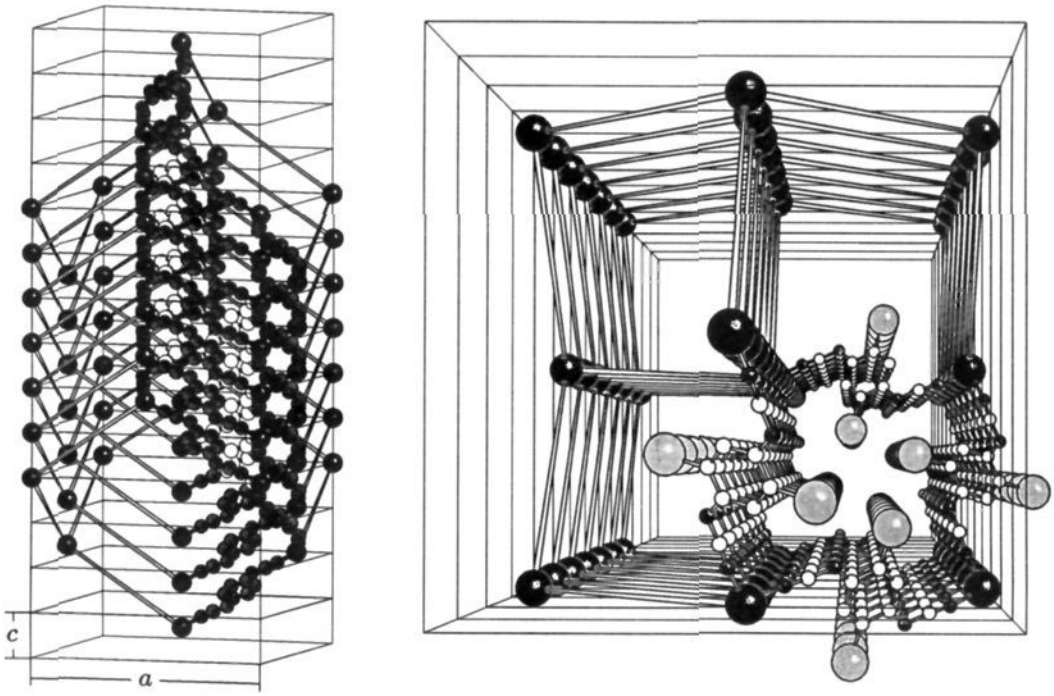

Figure 5. Part of the 7-fold diamondoid superstructure in the crystal lattice of (2,5-R^1,R^3–DCNQI)$_2$Cu (space group $I4_1/a$), formed by the intercalation of seven adamantanoid Cu_{10} clusters from Figure 4. In both figures, three-fourths of the ligands between the copper ions are replaced by "Cu–Cu bonds". Left: Side view perpendicular to the direction of stacking. The substituents R^1 and R^3 are not shown. Right: perspective view in the direction of stacking. The nonequivalence of the Cu–Cu distances is due to the chosen perspective.

are also met by the DCNQI copper salts **1** (above the phase transition); that is, we have an infinite three-dimensional lattice of indistinguishable mixed-valent ions (formally $Cu^{\delta+}$, $1 < \delta \leq 1.33$) bridged by the DCNQI molecules. Class III behavior is enabled since energetically the Cu d orbitals are positioned very close to the Fermi level of the ligand LUMO band. Hence, charge transfer (back-donation from the d^{10} metal center to the ligand LUMO) and conduction, respectively, can occur via the DCNQI bridges. The conductivity arising from this conduction path can be determined by observing an enhanced conductivity perpendicular to the stacking axis (reduced anisotropy $\sigma_\parallel/\sigma_\perp < 50$ as compared to $\sigma_\parallel/\sigma_\perp \approx 6000$ for the DCNQI non-copper salts).[1b,22b,36] Both conduction paths just described are coupled to each other in the copper salts **1** due to the participation of the DCNQI units in both paths ("two conductors in one"). Hence, CDW-induced phase transition will not occur as long as a delocalized class III state of the mixed-valent copper framework is energetically favored, as compared to a more or less localized class II state. Consequently, the metal–insulator phase transition in copper salts **1** corresponds to a class III → class II transition in terms of Robin–Day classification, along with the development of a charge density wave. This description is consistent with recent considerations of Kobayashi et al.[37] that the phase transition in copper salts **1** is a cooperative coincidence of static charge ordering (SCO) at the cation side (···$Cu^+Cu^+Cu^{2+}$···) and charge density wave (CDW) formation on the DCNQI columns, both only commensurate for a charge transfer rate $\rho \approx 0.63$. This interpretation is also in agreement with the observation of 3-fold superstructures in group M–I salts at low temperatures.[26]

From this point of view, the extreme sensitivity of copper salts **1** to changes in the coordination geometry around the copper ion becomes even more obvious, since "optimal" interaction, both in terms of relative energy and in terms of geometrical overlap of Cu 3d orbitals and the ligand LUMO band, is an essential prerequisite for the maintenance of class III behavior, that is, delocalization or rapid exchange of oxidation states.

In the following section the interrelation between the coordination angle α_{co} and the phase behavior just described will be discussed. As a consequence of the reduced symmetry (D_{2d}) of the coordination tetrahedron ($\alpha_{co} > 109°\ 28'$), the t_2 set of the Cu 3d orbitals, for ideal tetrahedral symmetry (T_d), is split into two groups; that is, the energy of the d_{xy} orbital is raised while that of the degenerate d_{xz} and d_{yz} orbitals is lowered (Figure 7). The amount of splitting ΔE depends on (1) the degree of tetragonal distortion (α_{co}), (2) the effective charge q of the ligands, (3) the relative energy of the Cu 3d orbitals and the Fermi level of the ligand LUMO band (reflected by ϵ_{LUMO}), and (4) the geometrical overlap between Cu 3d orbitals and the ligand LUMO band (reflected by the structural parameters α_{co}, d_{Cu-N}, and θ). From tight-binding band electronic structure calculations Kobayashi et al.[28a,c] established the following features: (1) If the splitting is rather small (low tetragonal compression), i.e. contribution of d_{xy}, d_{xz}, and d_{yz} orbitals to the pπ–d interaction, the system reveals more than two pairs of Fermi surfaces so that no single modulation wave vector can produce a gap all over the Fermi surfaces ("multi-Fermi surface" character). Hence, the system stays metallic down to the lowest temperatures. (2) If the splitting is large (high tetragonal compression), the pπ–d interaction is mainly determined by the d_{xy} orbital and the ligand LUMO band. In this case, the band structure becomes rather simple. Two pairs of Fermi surfaces can be nested into each other with the wave vector $k_z = c^*/3$, and an energy gap is created over the whole actual Fermi surface. Hence, the system undergoes a metal–insulator phase transition.[28a,c]

In order to obtain information about the dependence of the phase behavior on the nature of the substituents R^1 and R^3, calculated $\Delta E/q$ values for ambient temperature were correlated with the transition temperatures T_{M-I}.[28c] Although the correlation was excellent for salts which undergo phase transitions, it failed for the two metallic systems **1a** (Me/Me) (predicted $T_{M-I} \approx 127$

(36) Mori, T.; Imaeda, K.; Kato, R.; Kobayashi, A.; Kobayashi, H.; Inokuchi, H. *J. Phys. Soc. Jpn.* **1987**, *56*, 3429.

(37) Kato, R.; Sawa, H.; Aonuma, S.; Okano, Y.; Kagoshima, S.; Kobayashi, A.; Kobayashi, H. *Proceedings of the International Conference on Synthetic Metals*, Göteborg, Sweden; Synthetic Metals; Elsevier Sequoia: Lausanne, Switzerland, 1992.

(38) Albright, D. A.; Burdett, J. K.; Whangbo, M.-H. *Orbital Interactions in Chemistry*; John Wiley & Sons: New York, 1985; pp 304–309.

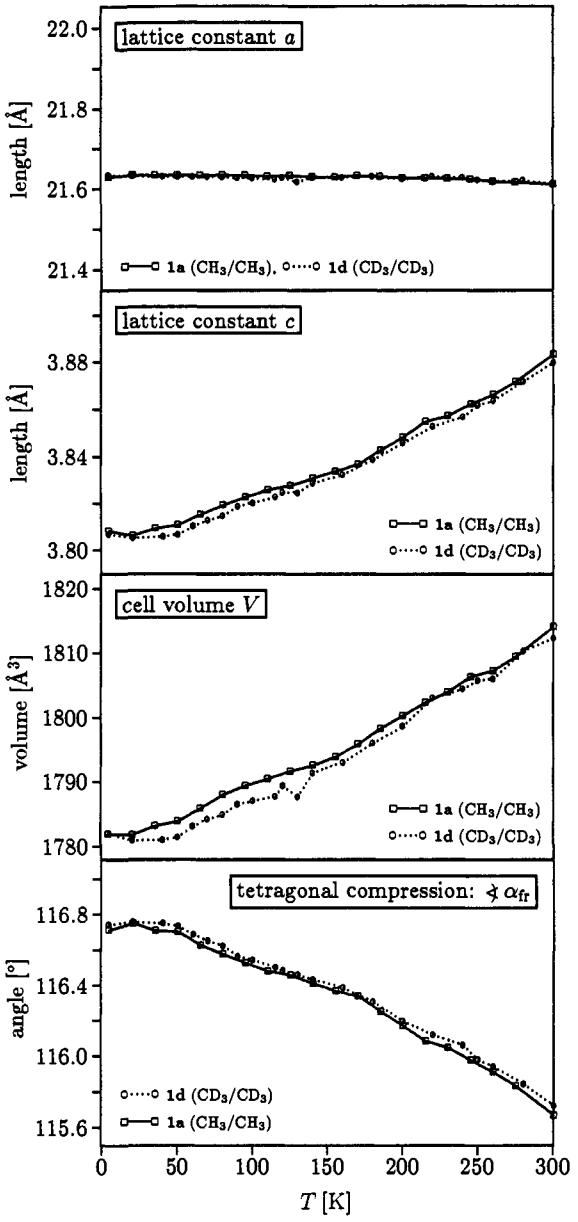

Figure 6. Temperature dependence of the lattice constants a and c (both windows show segments of the ordinate with comparable relative scales), of the unit cell volume V, and of the tetragonal compression (represented by the angle α_{fr}) for **1a** and **1d**.

K) and **1n** (OMe/OMe) (predicted $T_{M-I} \approx 166$ K). To some extent, this failure may be due to too rough assumptions: (1) The expressions used for the calculation of $\Delta E/q$ consider only the electrostatic effects, which neglect, for instance, the somewhat differing relative energies of Cu 3d orbitals and the Fermi level of the ligand LUMO band (depending on the substitution pattern), a feature that can be derived from the voltammetric half-wave potentials $E_{1/2}$ and the calculated AM1-LUMO energies of the DCNQI molecules, respectively. (2) $\Delta E/q$ as a measure for ΔE implies that q has the same value for all copper salts. Even assuming this will be the case, ESR data[39] and our results obtained from AM1 calculations[6,7] indicate that the π-spin population and the charge distribution, respectively, between the DCNQI core and the peripheral N—C≡N groups vary somewhat depending on the nature of the substituent combinations. The principal cause for failure may result from the neglect of other features depending on temperature and coordination geometry such as the influence of coupling between electronic and vibrational

(39) Gerson, F.; Gescheidt, G.; Möckel, R. *Helv. Chim. Acta* **1988**, *71*, 1665.

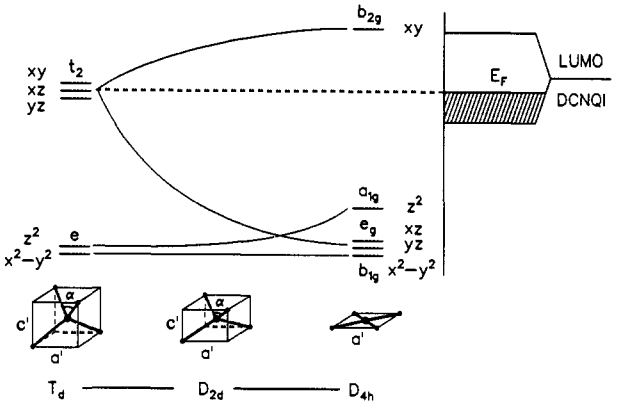

Figure 7. Bottom: Walsh diagram for the compression of a tetrahedral to a square planar ML_4 complex maintaining D_{2d} symmetry (according to ref 37). So far, only σ interactions are considered. Top: Schematic representation of the Fermi level of the ligand LUMO band.

motions (arising from molecular as well as lattice modes) on the charge exchange, i.e. on transport properties within the class III network of mixed-valent copper ions (vide infra). The exceptional behavior of **1n** (OMe/OMe) was attributed to a distinct difference in the overlap integral between the LUMO and the Cu d orbitals as compared to **1a** for instance, which was ascribed to the larger size of the methoxy group.[28c] However, as our renewed comparison[7] of all available structural data revealed, there are *discontinuous* changes in nearly all structural parameters of **1n** (OMe/OMe) and other methoxy-substituted copper salts which are mainly due not to the size of the methoxy group but to its *bent* (anisotropic) shape as compared to the case of the substituents (Cl, Br, I, also Me) with nearly *spherical* (isotropic) shape. Thus, methoxy-substituted copper salts should be discussed apart from the other salts.

Since the other coordination parameters are almost invariant (d_{Cu-N}) or vary only slightly (angle θ) for copper salts **1** with combinations of *spherical* substituents, the coordination angle α_{co} is the main determinant of the splitting ΔE and hence the phase behavior (metallic or semiconducting state). Therefore our approach will be a more phenomenological one.

As becomes obvious from the striking results presented above, phase transitions in salts **1** occur only if α_{co} exceeds a certain critical threshold.[1a,10] To estimate this threshold angle, we plotted the coordination angle α_{co} against the temperature for the copper salts **1** with *spherical* substituents (Figure 8). This plot is based on the following findings and considerations: (1) Values of α_{co} at ambient temperature and lower temperatures are available from X-ray data presented here and elsewhere.[6,28] A renewed examination[7] of all available structural data revealed that variations of α_{co} at ambient temperature (from 127.1° (**1m**, Cl/Cl) to 123.2° (**1f**, Me/I)) are driven by a combination of steric as well as electronic substituent effects; that is, increasing size of the substituents on the one hand and introduction of electron-releasing substituents (i.e. Me groups) on the other hand result in decreasing values for α_{co}. The influence of the electron-releasing substituents on α_{co} is ascribed to a redistribution of negative charge from the DCNQI core to the peripheral N—C≡N groups upon introducing these substituents (derived from results of AM1 calculations[6,7]) and therefore an enhanced Coulomb repulsion of the ligands around the copper ion.[7] Indeed, the room-temperature values of α_{co} can be reproduced with excellent accuracy by the two-parameter equation ($r = 0.993$)

$$\alpha_{co} = 1.34\alpha_{fr} + 3.89E_{1/2} - 31.79 \qquad (3)$$

Hereby, the steric effects are reflected by α_{fr}, since it depends only on the size of the substituents. The electronic effects are represented by the first voltammetric half-wave potentials $E_{1/2}$, which are linearly correlated to the negative partial charges (from

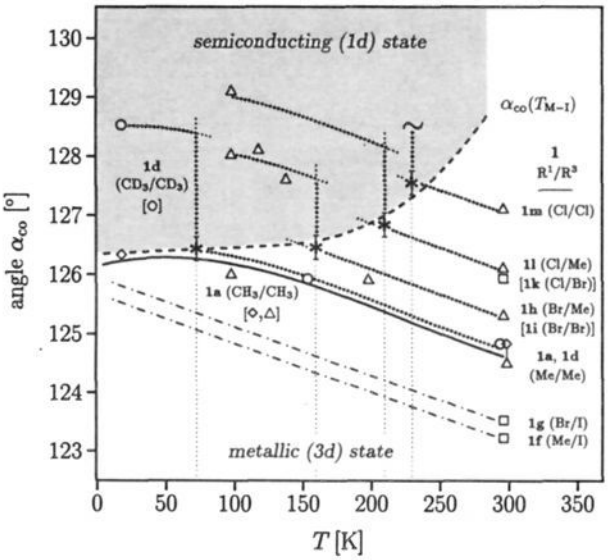

Figure 8. Plot of coordination angles α_{co} (∠N–Cu–N) in $(R^1,R^3$–DCNQI$)_2$Cu (**1**) versus temperature. Values (◇, ○, □, △) are obtained from X-ray analyses: (◇, ○) this work; (□) ref 6; (△) ref 28c. Since salts **1** with combinations of various *spherical* substituents reveal nearly the same tetragonal compressibilities upon cooling between room temperature and T_{M-I} (cf. refs 23, 28), the slopes of the evaluated plots of α_{co} versus T (···) starting from the known room-temperature values are assumed to be the same in this temperature range. The values of $\alpha_{co}(T_{M-I})$ (•) were obtained by cutting the just-mentioned branches of α_{co} versus T at the phase-transition temperatures T_{M-I}, which are known from temperature-dependent measurements of conductivities and lattice constants.[6,28] The hatched line (- - -) connecting the values of $\alpha_{co}(T_{M-I})$ (•) marks the border between the metallic and the semiconducting phase. For **1f** (Me/I) and **1g** (Br/I), α_{co} is predicted not to surpass the borderline, not even on the extreme assumption of α_{co} decreasing linearly over the whole temperature range (– · – · –). The temperature dependence of α_{co} below T_{M-I} is shown only in a very schematic way.

AM1 calculations) at the terminal nitrogen atom of the N—C≡N group. For this reason, **1a** (CH_3/CH_3, 124.8°) reveals a lower α_{co} value than **1i** (Br/Br, 125.3°), although the van der Waals volume of Br (25.1 Å^3)[8] is larger than that of the Me group (22.7 Å^3)[8] (cf. Figure 8). We assume that the linear correlation between α_{co} and α_{fr} will also be valid upon cooling, at least down to the phase-transition temperature T_{M-I}. (2) As the structural investigations of Kobayashi et al.[23,28] pointed out for salts **1** with the substituent combinations under consideration here, the plots of lattice constants a and c, and hence of α_{fr}, versus temperature have almost the same slopes above the phase transition. That is, the salts reveal nearly the same tetragonal compressibility upon cooling. (3) Phase-transition temperatures T_{M-I} are available from conductivity measurements and X-ray experiments presented by several groups.[6,28]

Following these considerations, a quite reliable evaluation of the development of α_{co} upon cooling is enabled (Figure 8), even for those salts for which only room-temperature values of α_{co} are available so far. The plots for **1k** (Cl/Br) and **1i** (Br/Br) (Figure 8: in parentheses), are not drawn explicitly since, within the uncertainty of this correlation, they resemble the curves of **1l** (Cl/Me) and **1h** (Br/Me), respectively (same values of α_{co} at room temperature and 100 K; similar values of T_{M-I}). Even taking into account some uncertainty within this correlation, the following features can be derived: (1) Interpreting Figure 8 as a phase diagram, the hatched line (---) connecting the values of α_{co} at the phase transition ($\alpha_{co}(T_{M-I})$) marks the border between the metallic and the semiconducting phase, respectively. Obviously, the slope of this borderline is not linear over the entire temperature range; i.e. it starts rather flat in the low-temperature region and becomes steeper with increasing temperature above 150 K. Besides contributions of other structural parameters influencing the geometrical overlap between Cu 3d orbitals and the ligand LUMO band (reflected in somewhat varying values for d_{Cu-N} and θ), this shift of $\alpha_{co}(T_{M-I})$ into the region of higher tetragonal compression (hence larger splitting ΔE) may probably be due to an increasing stabilization of the metallic state by temperature-dependent vibronic coupling (for instance, modulation of ΔE by molecular vibrations and/or lattice vibrations along and perpendicular to the direction of stacking). The close interdependence of charge transfer in mixed-valent compounds and coupling between electronic and vibrational motions was established by theoretical considerations of Piepho et al.[40] on the well-known Creutz–Taube ion as a model for Robin–Day class II and class III compounds. (2) According to our evaluations, $\alpha_{co}(T_{M-I})$ converges to a critical value at low temperatures ($\alpha_{co} \approx 126.4°$, corresponding to a value of $\alpha_{co} \approx 124.8°$ at ambient temperature) below which no phase transition will occur. Hence, copper salts that will not exceed this threshold value will remain metallic down to the lowest temperatures. This is demonstrated for the two metallic salts **1f** (Me/I) and **1g** (Br/I), for which the dependence of α_{co} and α_{fr} on temperature has not been investigated thus far.[41] These salts are predicted not to surpass the borderline, not even on the extreme assumption of a linearly decreasing angle α_{co} (– · – · –). (3) The phase diagram is useful to describe the phase behavior of **1** not only upon cooling and for different substituent patterns but also upon pressurizing. Applying pressure to a certain salt **1** means an upward shift of the corresponding α_{co} plot (flattening of the coordination tetrahedron) with the consequence of raising T_{M-I}. (4) The borderline position of **1a** ($CH_3/CH_3/H_2$) can clearly be seen from Figure 8. Its value of α_{co} at low temperatures (30–70 K) nearly touches the threshold value. Hence, the high-pressure sensitivity of **1a**, in general, and the reentrance behavior under low pressure, in particular, become obvious.

While the *discontinuous* change in the tetragonal compression observed for group M–I salts during the phase transition (Robin–Day class III → class II) was attributed to a Jahn–Teller-type distortion,[23a] the question still remains open whether the *continuously* increasing tetragonal compression above T_{M-I} is also due to a (temperature-dependent) Jahn–Teller effect or whether this is a common feature of all DCNQI metal salts with structures isomorphic with $I4_1/a$, possibly due to temperature-dependent packing or lattice vibrational effects. Hopefully, further experiments[41] on DCNQI metal salts (M = Li, Ag) concerning the *temperature dependence of the crystal structures will provide an* answer to this question.

Conclusions

The unprecedented strong secondary deuterium isotope effect of $(Me_2$–DCNQI$)_2$Cu, which was reflected in conductivity and susceptibility measurements as well as ESR spectroscopy and X-ray investigations, illustrated that metallic **1a** ($CH_3/CH_3/H_2$) is a borderline case since its ligand coordination angle at low temperatures is very close to a proposed threshold angle $\alpha_{co} \approx 126.4°$ above which a phase transition to a strictly one-dimensional semiconductor occurs.

On the basis of the analysis of the 7-fold diamondoid superstructure within the crystal lattice of copper salts **1**, a metal–semiconductor phase diagram was provided by a correlation of coordination angles α_{co} with the temperature. This phase diagram provides an overall description of the phase behavior of copper salts **1** with a combination of *spherical* substituents with respect to several features: behavior upon cooling, pressurizing, and varying the substituents.

(40) (a) Piepho, S. B. *J. Am. Chem. Soc.* **1990**, *112*, 4197. (b) Piepho, S. B. *J. Am. Chem. Soc.* **1988**, *110*, 6319. (c) Piepho, S. B.; Elmars, R. K.; Schatz, P. N. *J. Am. Chem. Soc.* **1978**, *100*, 2996.

(41) X-ray investigations on the temperature dependence of α_{co} are in progress for **1f** (Me/I) and **1g** (Br/I) as well as for DCNQI metal salts with M = Li, Ag: Hemmerling, M. Ph.D. Thesis, University of Würzburg, in preparation.

Novel insight into the unique role played by the copper ions in the copper salts **1** is given by describing the salts as a combination of a common segregated-stacks conductor and a Robin–Day class III conductor. Considering the class III character of the copper framework and the temperature dependence of the borderline angle $\alpha_{co}(T_{M-I})$ within the metal–semiconductor phase diagram, new questions arise concerning the role of vibronic coupling in the stabilization of the metallic state, which have not been mentioned so far.

Experimental Section

Starting Materials and Crystal Growth.[2a] Deuterated 2,5-Me_2–DCNQIs were synthesized according to common methods[7,42] and are reported elsewhere. All compounds provided the expected spectroscopic and analytical data. The grade of deuteration of the DCNQIs was determined by ^{1}H-NMR spectroscopy (250 MHz) and confirmed by mass spectroscopy: **1b** (ring-D > 95%); **1c** (methyl-D > 99%); **1d** (methyl-D > 99%); **1e** (methyl-D > 99%, ring-D > 97%). Single crystals of [2,5-R^1,R^3–DCNQI]$_2$Cu were obtained by galvanostatic electrolysis of acetonitrile solutions of 2,5-R^1,R^3–DCNQI and $[Cu(CH_3CN)_4]ClO_4$ in a U-shaped electrolysis cell under argon atmosphere. Microcrystalline materials for X-ray powder diffraction were obtained by adding acetonitrile solutions of CuI to boiling solutions of 2,5-R^1,R^3–DCNQI in acetonitrile under argon atmosphere, according to ref 42.

Solid-State Properties.[2b,c] The conductivity measurements were performed by conventional four-probe techniques. Cooling was achieved by a Helium flow cryostat (Oxford CF 1204), and temperature control, by an ITC-4 (Oxford). Our ESR machine (Varian E-line Century Series) was equipped with an Oxford ESR-900 continuous-flow cryostat. The total susceptibility was measured by a SQUID (magnet property measurement system Fa. Quantum design).

Structure Determinations.[2d,e] Diffraction data for **1a** (298, 20 K) and **1d** (298, 20 K) were collected on a four-circle Huber diffractometer equipped with a closed-cycle helium refrigerator. The crystal was cooled over a period of 3 h to 20(5) K. Accurate unit cell parameters at both temperatures were obtained by least-squares refinement of 40 centered reflections and are listed in Table I together with other details of data collection and structure refinement. Intensity data were collected with the $\theta/2\theta$ step scan technique up to a maximum of 60°. Three standard reflections were measured after every 97 reflections, which showed no systematic variations. Corrections for Lorentz and polarization effects were made, and an empirical absorption correction was applied using the ψ-scan procedure.

Data collection at 156 K was carried out on a Picker/Crystal-Logic four-circle diffractometer using the $\theta/2\theta$ step scan technique and Mo Kα radiation (graphite monochromator, λ = 0.710 69) (details in Table I). The sample temperature was obtained with the use of a cold N_2 stream.[44] Unit cell parameters were obtained from least-squares refinement of 30 centered reflections.

The position of the copper atom was determined from the Patterson map, and the positions of the remaining atoms including the hydrogen atoms were obtained from difference Fourier maps. The structures were refined to the agreement factors shown in Table I using the UCLA crystallographic package.[45] Atomic coordinates and anisotropic displacement parameters are listed in Tables II–VI. Selected interatomic distances and angles are listed in Table VII.

Temperature Dependence of Lattice Constants.[2f,g] Lattice constants of **1a** and **1d** between 4 and 300 K were determined by X-ray powder diffraction methods using a Siemens D500 diffractometer with Co Kα radiation (secondary graphite monochromator) equipped with an Oxford He-flow cryostat. The Ge(111) reference peak was used as an internal standard. Step scan data with a scan width of 0.02° in 2θ and 3-s counting time per step were collected in the range 29.5–38.3° 2θ, which contains the reflections 260, 031, 321, 411, 460, 341, and 251. Unit cell parameters were refined by profile refinement (Hill and Howard[46]), and the strongly preferred orientation effects of the investigated Cu salts were corrected according to Dollase.[47]

Acknowledgment. This work was supported by the Fonds der Chemischen Industrie, by the Volkswagen-Stiftung, by the Deutsche Forschungsgemeinschaft (Grant SFB 329), and by the JCPDS/International Center for Diffraction Data (Grant-in-Aid 90-03 to E.T.). T.M. thanks the Deutsche Forschungsgemeinschaft for a research grant. We also thank Prof. C. E. Strouse for the use of the ultralow-temperature diffractometer.

Supplementary Material Available: Tables of complete crystal data, fractional atomic coordinates, anisotropic thermal parameters, bond lengths, and bond angles (18 pages); listings of observed and calculated structure factors (29 pages). Ordering information is given on any current masthead page.

(42) Aumüller, A.; Hünig, S. *Liebigs Ann. Chem.* **198**, 142.
(43) Aumüller, A. Ph.D. Thesis, University of Würzburg, 1985.
(44) Strouse, C. E. *Rev. Sci. Instrum.* **1976**, *47*, 871.
(45) The programs used included modified versions of the following programs: REDUCE (Broach, Coppens, Becker, and Blessing), peak profile analysis, Lorentz and polarization corrections; ORFEE (Busing, Martin, and Leavy), distance, angle, and error calculations; ORTEP (Johnson), figure plotting. Scattering factors and corrections for anomalous dispersion were taken from: *International Tables for X-ray Crystallography*; Kynoch Press: Birmingham, England, 1974; Vol. IV.
(46) Hill, R. J.; Howard, C. J. Report No. M112; Australian Atomic Energy Commission, Lucas Heights Research Laboratories: Menai, NSW, Australia, 1986.
(47) Dollase, W. A. *J. Appl. Crystallogr.* **1986**, *19*, 267.